metals

MDPI

Article

Cracking during High-Temperature Deformation of a High-Strength Polycrystalline CoNi-Base Superalloy

Daniel Hausmann [1,*], Lisa Patricia Freund [1], Cecilia Solís [2], Sven Giese [1], Mathias Göken [1], Ralph Gilles [3] and Steffen Neumeier [1]

[1] Department of Materials Science & Engineering, Institute I: General Materials Properties, Friedrich-Alexander-Universität Erlangen-Nürnberg, 91058 Erlangen, Germany
[2] German Engineering Materials Science Center (GEMS) at Heinz Maier-Leibnitz Zentrum, Helmholtz-Zentrum Hereon, 85748 Garching, Germany
[3] Heinz Maier-Leibnitz Zentrum, Technische Universität München, 85748 Garching, Germany
* Correspondence: daniel.dh.hausmann@fau.de

Abstract: The crack susceptibility during processing has a crucial influence on the workability of wrought alloys. In particular, the processing of high-strength alloys that are prone to cracking is challenging and various process parameters have to be optimized to achieve a good formability. The polycrystalline CoNi-base superalloy CoWAlloy1 provides a high potential for high-temperature applications due to it having a large forging window, a high γ' fraction and excellent creep properties. In order to study its formability during hot rolling, its deformation behavior and susceptibility to cracking were characterized by sub- and supersolvus compression tests at temperatures between 1000–1150 °C. At temperatures around the γ' solvus temperature, no cracks formed during the compression testing, while at lower temperatures, cracking occurred. Additionally, an in-situ high-temperature small-angle neutron scattering revealed the phase fractions and the precipitate size distributions at different processing temperatures. It was found that a high fraction of γ' forms during cooling and cracking starts at the surface of the bar, when the hot bar encounters the cold rolls during hot rolling. Apparently, the precipitation of γ', which causes a high strength and reduced ductility, and the absent recrystallization leads to pronounced crack propagation and limited formability below the γ' solvus temperature.

Keywords: compositionally complex alloy; Co-base superalloy; small-angle neutron scattering; scanning electron microscopy; crack propagation; workability

Citation: Hausmann, D.; Freund, L.P.; Solís, C.; Giese, S.; Göken, M.; Gilles, R.; Neumeier, S. Cracking during High-Temperature Deformation of a High-Strength Polycrystalline CoNi-Base Superalloy. *Metals* **2022**, *12*, 1520. https://doi.org/10.3390/met12091520

Academic Editor: Lei Zheng

Received: 22 July 2022
Accepted: 11 September 2022
Published: 14 September 2022

1. Introduction

There are huge efforts to develop new alloys with similar or better mechanical properties than the state-of-the-art high-strength wrought alloy Udimet 720Li (U720Li). In the focus of the production of newly developed alloys is also their improved workability. Several studies have investigated the hot workability of superalloys by conducting compression tests at high temperatures and different strain rates [1–4]. Recently, Aubert and Duval developed novel wrought Ni-base superalloys with a good combination of costs, workability and mechanical properties [5]. The alloy AD730 provides a higher workability than Waspaloy and U720Li do. Its tensile and creep properties are significantly higher than those of ATI 718Plus and slightly higher than U720Li [6]. Similarly, VDM Metals recently developed the VDM® Alloy 780 to obtain a comparable forging window to that of Inconel 718 (IN718), but with superior microstructural stability, which allows significantly higher service temperatures [7,8]. VDM® Alloy 780 shows a high tensile strength at room temperature and it has excellent mechanical strength at elevated temperatures [9].

Other potential candidates for new wrought alloys are the compositionally complex, γ'-strengthened CoNi-base superalloys that are based on the Co-Al-W system. These were developed in recent years and reveal promising mechanical properties [10–14]. The

polycrystalline superalloy CoWAlloy1 has a very good high-temperature strength and excellent creep properties due to a high γ' precipitate fraction and a high γ/γ' lattice misfit. A large gap between the γ' solvus and solidus temperature provides a high potential for high-temperature applications as a wrought alloy. $L1_2$-ordered γ' $(Co, Ni)_3(Al, W, Ti, Ta)$ precipitates are embedded in an CoCrNi-rich γ matrix and they strengthen the alloy. However, CoWAlloy1 has a limited workability when it is compared to that of its related alloys CoWAlloy2 [15], CoWAlloy3 [16] or CoWAlloy6 [16] at low temperatures. It seems that the γ' solvus temperature has an effect on cracking and the formability during high-temperature deformation.

Different approaches have been developed to model the fracture, hot deformation behavior and workability of metals [17,18]. The simulation of the microstructural evolution [19–21] during the forging or rolling process is an important method to predict the workability of superalloys. A temperature gradient appears within the forged billet or the rolled bar due to the heat transfer between the hot superalloy and the cold dies or rolls. This temperature gradient is crucial for understanding the forging or rolling process and it influences the microstructural evolution. Dandre et al. [22] simulated the temperature profile of a deformed IN718 billet during ingot-to-billet conversion with an initial temperature of 1120 °C. The forged material had a temperature of about 1040 °C at the surface, whereas the temperature in the core of the billet was above 1120 °C. Therefore, if the precipitation of a strengthening or a grain boundary pinning phase occurs, this will initiate near the surface of the deformed bar due to the lower temperature. This leads to a locally increasing strength and worse formability. Zhang et al. [23] mentioned that a recrystallized microstructure, i.e., a uniform and fine grain structure, facilitates good formability at high temperatures. It was shown that dynamic recrystallization takes place in the easily deformed zones with a uniform microstructure, and recrystallization leads to a better formability.

In this study, the formability of CoWAlloy1 during high temperature deformation was investigated by conducting compression tests at 1000–1150 °C and strain rates of 10^{-2} s^{-1} and 10^{-3} s^{-1}. Scanning electron microscopy (SEM) was used to characterize the microstructure after the deformation at high temperatures. In-situ high-temperature small-angle neutron scattering (SANS) was conducted to analyze the precipitate size distributions and the phase fractions at different processing temperatures. SANS has been shown to be a very powerful method to analyze the different fractions and sizes of the γ' precipitates [24–29]. The aim of this study is to clarify the reasons for the reduced formability and cracking of CoWAlloy1.

2. Materials and Methods

2.1. Observations during Hot Rolling

To characterize the varying formability of the CoWAlloy series, ingots of the different alloys were homogenized at 1250 °C for 3 h and then heated up for 1 h at 1100–1200 °C, before rolling. Bars of the alloys with an initial diameter of 40 mm were rolled in several steps including during intermediate heating on a non-heated rolling mill with a starting temperature of 1100 °C at the company Vacuumschmelze GmbH (Hanau, Germany). CoWAlloy1 was only rolled down to a final diameter of 36 mm, whereas the similar alloys, CoWAlloy2 [15], CoWAlloy3 [16] and CoWAlloy6 [16], could be rolled down to a diameter of 15 mm without the appearance of any surface cracks even at lower deformation temperatures because they had a better formability.

2.2. Experimental Methods

Table 1 gives the chemical composition of the alloy under investigation in this study, named CoWAlloy1.

The alloy was vacuum arc melted from raw elements, cast, and homogenized for 3 h at 1250 °C at the company Vacuumschmelze GmbH (Hanau, Germany). Compression tests were performed on cylindrical samples of the homogenized material with a diameter of 6 mm and a length of 9 mm, which were manufactured by wire spark erosion (Mechanikw-

erkstatt FAU, Erlangen, Germany). To achieve the parallel surfaces, the samples were ground afterwards. The compression tests were executed using an electromechanical Instron 4505 testing machine (Instron, Norwood, MA, USA) at strain rates of 10^{-2} s^{-1} and 10^{-3} s^{-1} until reaching a total strain of 50%. The true stress and the true plastic strain were calculated from the recorded data and an effect of the friction between the specimens and dies was not considered, although barreling occurs at larger deformation. However, a friction effect on the stress–strain curves is negligible small at these conditions [30]. The material was heated up to 1100 °C and 1200 °C for 30 min before conducting the compression tests at temperatures of 1000–1150 °C in order to apply a similar heat treatment procedure as in the rolling process.

Table 1. Nominal alloy composition of CoWAlloy1 in %.

Element	Co	Ni	Al	W	Ti	Ta	Cr	Si	Hf	Zr	B	C
CoWalloy1	42.2	32.0	6.0	3.0	2.5	1.5	12.0	0.4	0.1	0.01	0.08	0.08

The microstructures of the deformed samples were investigated by using an SEM Zeiss Crossbeam (Zeiss, Oberkochen, Germany) 1540 EsB in conjunction with a back-scattered electron detector and an acceleration voltage of 20 kV at an 8 mm working distance. The samples were cut, ground, and polished up to 1 µm, and in a final step, they were polished with colloidal silica. The fraction of the crack area was analyzed from microstructural images using the software package ImageJ 1.53 (Bethesda, Maryland, USA) [31]. The visible crack area was compared to the total sample area. The thickness of the formed oxide layer was measured to characterize the oxidation behavior. The samples were annealed at 1100 °C and 1200 °C for 1 h to investigate the influence of the pre-heating temperature on the formation of oxides and the subsequent compression testing.

In-situ heat treatments were performed using the small-angle neutron scattering beamline SANS-1 (MLZ, Garching, Germany) [32] at the Heinz-Maier-Leibnitz Zentrum (FRM II) of the TU München due to the difficult determination of the γ' precipitate size and volume fraction by using electron microscopy techniques. Neutrons provide the advantage of average size and volume fraction determination over a large illuminated sample volume (here these are in the order of >100 mm^3) at elevated temperatures. Especially, the high penetration depth of the neutrons allows such experiments on real bulk samples [33]. Discs with a diameter of 15 mm were cut from the homogenized samples, which were ground to achieve parallel surfaces and a thickness of 1 mm. Data from three detector configurations were measured and combined to produce one SANS spectrum and to cover a maximum q-range. The detector distance was varied between 2, 8, and 20 m. The scattering measurements were performed with a beam diameter of 8 mm and a wavelength of 6 Å for the detector distances of 2 and 8 m and 12 Å at the detector distance of 20 m. In-situ measurements were performed with an implemented high-temperature vacuum furnace (MLZ, Garching, Germany). The homogenized sample was heated up to 1075 °C, where the scattering measurement lasts for 30 min. Thereafter, the sample was cooled down to 750 °C and was subsequently, again, investigated. The scattering patterns were analyzed, corrected for the background scattering from the furnace, calibrated with water measurements to an absolute intensity scale and merged with the software BerSANS 14-Aug-2014 (Darmstadt, Germany) [34]. The data was fitted with the software SASfit 0.94.11 (Villingen, Switzerland) [35]. The γ' precipitates were modeled as spherical particles with a log-normal distributed particle size, and a Porod function was used for the background correction. The scattering contrasts of the secondary and tertiary γ' precipitates and the surrounding γ matrix were calculated by using their chemical compositions, which were determined by using atom probe tomography (APT) (Cameca Instruments, Madison, Wisconsin, USA) [36]. The resulting scattering contrast of the secondary γ' precipitates is 1.18×10^{10} cm^{-2} and of the tertiary γ' precipitates is 8.28×10^{9} cm^{-2}.

An overview of the experimental methods is given in Figure 1.

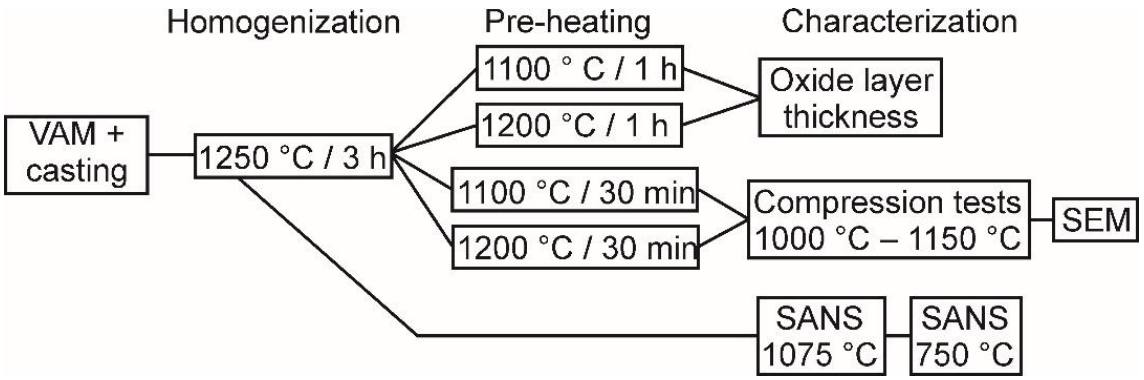

Figure 1. Schematic overview of the experimental methods and their sequence.

3. Results

3.1. Initial Homogenized Condition

Figure 2 shows an SEM image of the initial condition of the CoWAlloy1, which was heat treated at 1250 °C for 3 h. The initial condition has a homogenized microstructure and a median grain size of about 203 ± 34 µm. A slight residual segregation of the elements on the dendrite scale is still present.

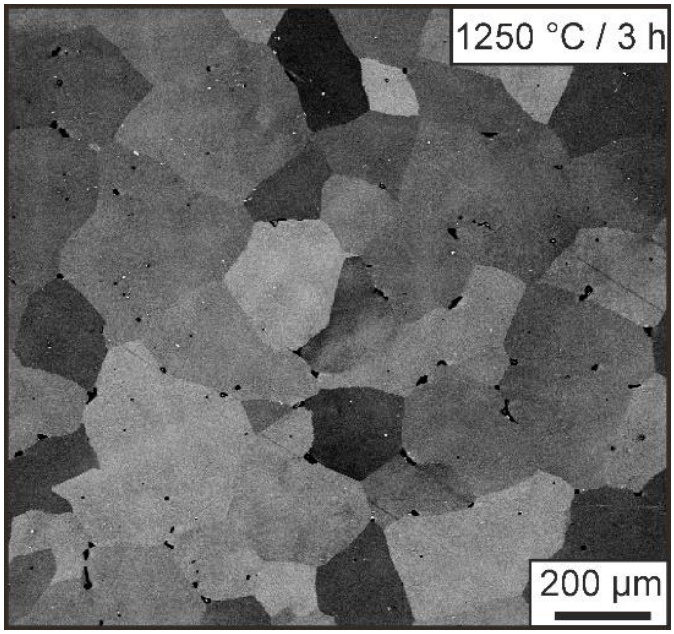

Figure 2. SEM image of the homogenized microstructure of CoWAlloy1 after a heat treatment at 1250 °C for 3 h.

3.2. Mechanical Properties during High Temperature Deformation

Compression tests were performed at elevated temperatures on this initial condition to determine the mechanical properties during the high-temperature deformation of CoWAlloy1. The specimens were subjected to different pre-heating temperatures before the specimens were tested at various strain rates and temperatures. The results of the compression tests with different strain rates are shown and briefly described in the Supplementary Material. Figure 3a shows the true stress as a function of the true plastic strain at a strain rate of 10^{-3} s^{-1} and for varying pre-heating temperatures. Moreover, macroscopic images of the samples after the compression tests at the different testing temperatures are shown Figure 3b.

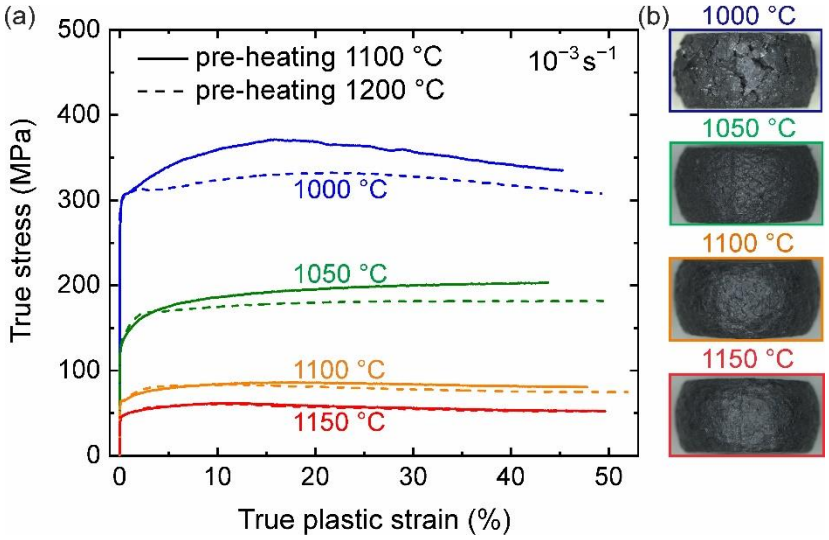

Figure 3. (**a**) True stress as a function of the true plastic strain at a strain rate of 10^{-3} s^{-1} and different pre-heating temperatures. (**b**) Macroscopic images of the samples after deformation at a strain rate of 10^{-3} s^{-1} and a pre-heating temperature of 1100 °C.

The strength decreases with increasing testing temperature. CoWAlloy1 has a yield strength of about 350 MPa at a testing temperature of 1000 °C, whereas it is just about 50 MPa at 1150 °C. After a short period of work hardening, a constant plastic deformation is noticeable at high testing temperatures. In contrast, the compression test of the specimen that was pre-heated at lower temperatures and tested at 1000 °C reveals that there was hardening until 15% strain, and a subsequent softening. The difference between both pre-heating temperatures is relatively small at higher testing temperatures. However, the higher pre-heating temperature leads apparently to less strengthening. No differences can be noticed especially at higher testing temperatures. The sample, after deformation at 1000 °C, reveals a surface with a lot of deep cracks (Figure 3b). Massive damage at the rim area of the deformed sample occurred. A lower amount of cracks and smaller cracks occurred with an increasing testing temperature. This indicates that there is a limited workability for the material at lower temperatures and a better formability with almost no cracks at higher testing temperatures.

3.3. Cracking during High-Temperature Deformation

More details of the deformed microstructure are revealed by the SEM images of the tested samples. The microstructures of the samples with a pre-heating temperature of 1100 °C are shown in Figure 4. The samples were deformed with a strain rate of 10^{-3} s^{-1} to a total strain of 50%. CoWAlloy1 has a deformed microstructure with a high amount of cracks at a testing temperature of 1000 °C. The cracks are all over the surface, which grow deep into the material and damage it (Figure 4a). The temperature at the given degree of deformation is insufficient for recrystallization, and therefore, a typical deformation structure can be noticed. The only recrystallized areas are at the grain boundaries and in the vicinity of the crack tips (Figure 4b,c). After compression tests at a temperature of 1150 °C, the microstructure is fully recrystallized, and a typical homogeneous grain structure is formed (Figure 4d). The higher deformation temperature is sufficient for recrystallization and with this, almost no or only small cracks appear at the surface (Figure 4e,f). Both conditions reveal the γ' phase after the compression tests (Figure 4c,f). However, the SEM images represent the condition at room temperature after cooling down from 1000 °C or 1150 °C. This temperature gradient and period of time for cooling is enough for the precipitation of the γ' phase, which is not present at the temperatures above the γ' solvus temperature.

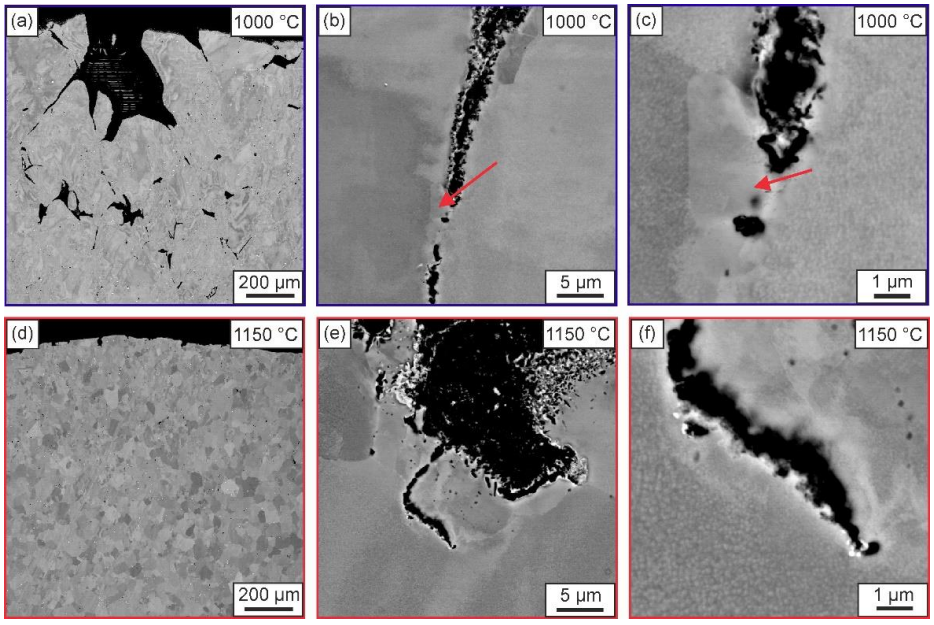

Figure 4. SEM images of the samples after deformation at a pre-heating temperature of 1100 °C, a strain rate of 10^{-3} s^{-1} and a testing temperature of (**a**–**c**) 1000 °C and (**d**–**f**) 1150 °C. Red arrows indicate the partly recrystallized areas at the grain boundaries.

Figure 5 illustrates the quantitative determination of the crack area after deformation, where the crack area fraction is plotted over the testing temperature. All conditions reveal no obvious surface cracks at a testing temperature of 1100 °C and above, whereas cracks or at least small cracks can be found at 1050 °C and below. The crack area fraction decreases with increasing testing temperatures. The highest crack area fraction of about 5% is measured at a testing temperature of 1000 °C and the higher pre-heating temperatures. Above a threshold value of about 0.8% crack area fraction, cracks can be visually seen after the deformation, whereas no cracks are noticeable below this threshold value.

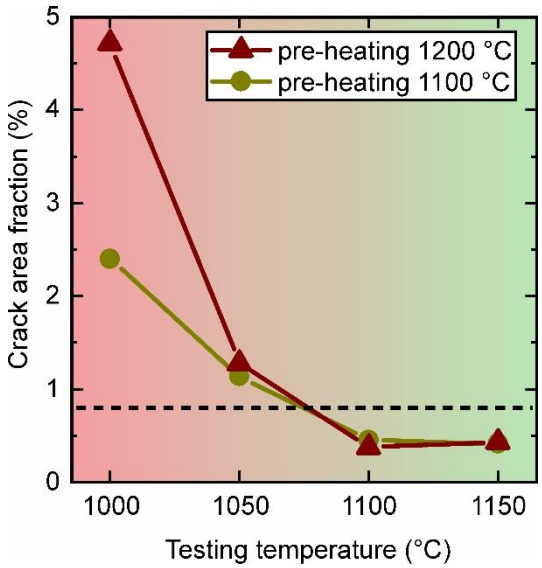

Figure 5. Crack area fraction as a function of the testing temperature after deformation at a strain rate of 10^{-3} s^{-1} and total deformation strain of 50%. The dashed line indicates a threshold value for the qualitative characterization of the samples. Below this threshold value no cracks could be observed visually at the surface inspection.

3.4. Oxidation

Additional annealing heat treatments were conducted at 1100 °C and 1200 °C for 1 h to characterize the oxidation behavior of CoWAlloy1. The results of this investigation can be seen in Figure 6.

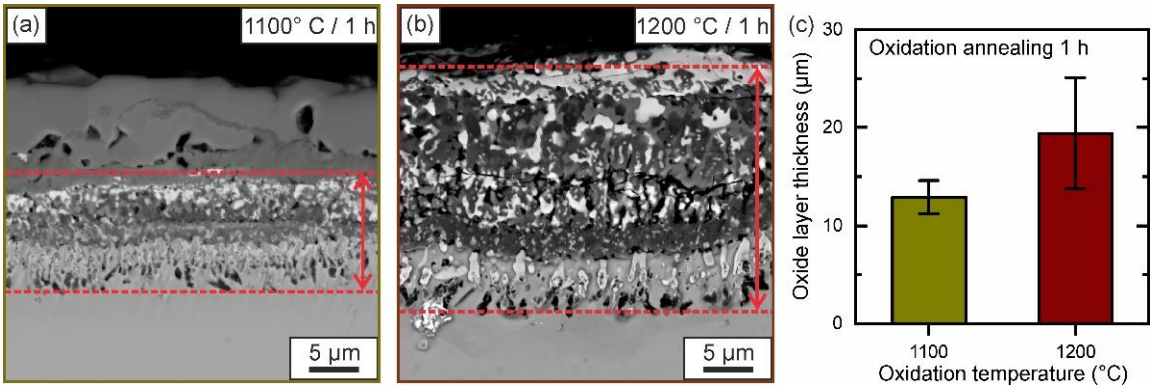

Figure 6. SEM images of the oxide layer after annealing at (**a**) 1100 °C/1 h and (**b**) 1200 °C/1 h. (**c**) Thickness of the inner oxide layer and the interlayer at different oxidation temperatures. The red dashed lines indicate the measured thickness of the inner oxide layer. The outer oxide layer was not included in the measurement due to severe spallation after annealing at 1200 °C for 1 h.

Different oxide layers form at both annealing temperatures. The innermost oxide phase is finger shaped and it is an Al-oxide, which has been confirmed by EDS measurements. The biggest difference between both oxidation temperatures is the thickness of the interlayer, which consists of different oxide types. A coarse-grained outer layer can be seen at 1100 °C (Figure 6a), whereas no or only a small amount of this outer layer exists at 1200 °C. The EDS measurements reveal that Co- and Ni-oxides form the outer layer. It seems that the outer layer was spalled off during the oxidation and subsequent cooling or during the sample preparation process (Figure 6b). Accordingly, the oxide thickness was determined only by including the inner and the interlayer for a better comparability. Figure 6c reveals a significantly thicker oxide layer at an annealing temperature of 1200 °C compared to a thinner oxide layer at 1100 °C.

3.5. Neutron Scattering Measurements around the γ' Solvus Temperature

The SANS measurements were conducted to determine the γ' precipitate size distributions and volume fractions above or below the γ' solvus temperature. The absolute macroscopic scattering cross section $d\sum/d\Omega$ as a function of the scattering vector q is plotted in Figure 7. The scattering curves at a temperature of 1075 °C and subsequent cooling down to 750 °C are compared.

The scattering curve, after heating the material to 1075 °C, has the shape of a Porod function, which is usually used to subtract the background or the very large particles of an SANS measurement. This indicates that there is only the measured background and no or a negligible amount of γ' precipitates due to the equality of the measured data points and the Porod function. After cooling down to 750 °C, the scattering curve takes the typical shape of a condition with a bimodal γ' precipitate size distribution. The curve can be fitted with two partial curves representing the secondary and tertiary γ' precipitates. The temperature gradient and time for precipitation during cooling is sufficient to form a noticeable γ' volume fraction of about 62%. Electron microscopy reveals a high γ' volume fraction of about 78% in the fully heat-treated condition of CoWAlloy1. The determined precipitate sizes and volume fractions of the secondary and tertiary γ' precipitates are summarized in Table 2.

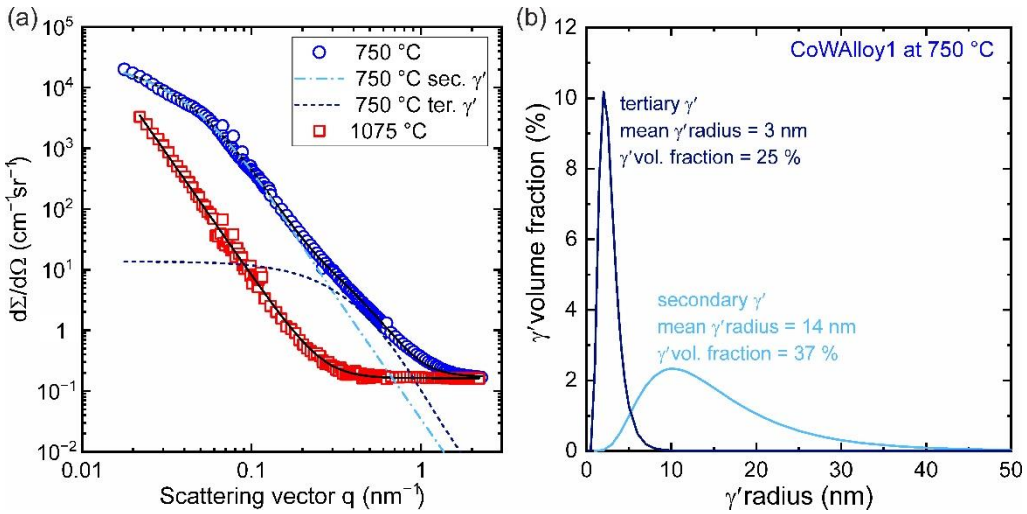

Figure 7. (**a**) SANS scattering curves of CoWAlloy1 at 1075 °C and after cooling down to 750 °C. The measurement after 750 °C consists of the log-normal distributed secondary and tertiary γ′ precipitate contributions. (**b**) The obtained log-normal size distributions of the precipitates at 750 °C.

Table 2. Mean radius r and volume fraction f of secondary and tertiary γ′ precipitates after cooling to 750 °C as determined by using small-angle neutron scattering (SANS). The width parameter σ represents the broadness of the γ′ log-norm size distributions and the standard deviation.

Condition	Secondary γ′			Tertiary γ′			Total γ′
	r/nm	σ/nm	f/%	r/nm	σ/nm	f/%	f/%
750 °C	13.6	0.5	37	2.5	0.4	25	62

4. Discussion

The CoWAlloy1 has an increased strength and a high amount of cracks which form during deformation when the present temperature is too low. This depends on the deformation rate, as the deformation rate has an influence on the strength and work hardening behavior of the alloy, the contact duration between the material and the rolls or dies and thus, the temperature distribution in the material, etc. The used strain rates of the compression tests are rather low when they are compared to those of the deformation rates present during rolling and forging, nevertheless, the conducted compression tests at the used parameters provide interesting insights in the alloy's formability. Apparently, the susceptibility for cracking increases below a critical temperature. The SANS measurements revealed the precipitation of the γ′ phase below this temperature, i.e., the γ′ solvus temperature. Accordingly, the limited formability of CoWAlloy1 below its γ′ solvus temperature of 1070 °C [36] seems to be explained by the strengthening effect of the γ′ phase and the lack of recrystallization.

When the hot bar encounters the cold rolls during hot rolling, the cracking starts at the surface of the bar. A simple approach of a diffusion profile of two semi-infinite bodies, which are in contact, can be used to simulate the temperature profile of the material during the rolling process. Equation (1) describes the temperature T_ξ at the distance to the surface ξ, [37]:

$$T_{\xi,t} = \frac{T_R + T_M}{2} - \frac{T_R - T_M}{2} ERF\left(\frac{\xi}{2\sqrt{\lambda_T \cdot t}}\right), \quad (1)$$

T_R is the temperature of the roll, T_M is the temperature of the rolled material, λ_T is the thermal conductivity and t is time. A thermal conductivity of 29.2 W/mK is assumed, which corresponds to the value of the Co-base superalloy Haynes25 at 1000 °C [38]. The

calculation is shown in Figure 8, where the temperature T_ξ is plotted over the distance to the surface after 1 s of contact.

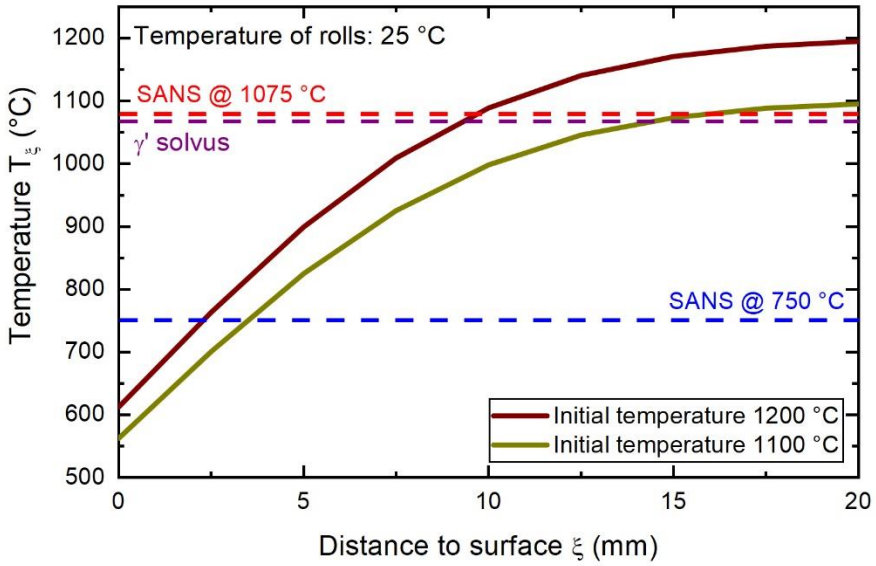

Figure 8. Calculated temperature profile of the bar during hot rolling and contact of the bar with the roll after 1 s of contact. The assumed temperature of the roll is 25 °C. The γ′ solvus temperature as well as the temperatures at which the SANS measurements were conducted are indicated by the dashed lines.

The temperature decreases close to the contact point of the material surface with the rolls. The temperature towards the contact point of the rolls and the rolled material is a factor of about two lower as that which is in the material core. Material with an initial temperature of 1200 °C or 1100 °C has a temperature of about 600 °C or 550 °C after 1 s of contact at the contact point, and then the temperature falls below the γ′ solvus temperature at a distance of about 0.9 cm or 1.5 cm to the surface. The low temperatures at the rim of the bar during rolling causes the massive precipitation of the γ′ phase. The SANS measurements revealed a very high precipitate fraction of 62% due to it cooling to 750 °C. Therefore, the formability is deteriorated due to the strengthening of the γ′ precipitates and the reduced ductility and cracking starts near the surface region, like the specimen that was compressed at 1000 °C (Figure 3b), which was also below the γ′ solvus temperature. This also explains the better formability of CoWAlloy2, 3 and 6, since their γ′ solvus temperatures, see Table 3 [36], and the strengths of their γ/γ′ microstructures are significantly lower than that of CoWAlloy1. The γ′ solvus temperature of CoWAlloy1 is about 40–80 °C higher than the solvus temperatures of the derivate alloys. Therefore, less precipitation and less strengthening occur during hot rolling at the rim of the bar of the derivative alloys.

Table 3. Determined γ′ solvus temperatures of CoWAlloy1, 2, 3 and 6 [36].

Alloy	γ′ Solvus Temperature/°C
CoWAlloy1	1070
CoWAlloy2	1030
CoWAlloy3	1006
CoWAlloy6	986

However, the question that considers why the specimens that were pre-heated for 1 h at the higher pre-heating temperature of 1200 °C show more cracking during subsequent compression at temperatures below the γ′ solvus temperature remains. To understand this, the influence of the pre-heating temperature on the oxidation behavior was also

characterized. In general, brittle oxides and the embrittlement of the grain boundaries can lead to a pronounced cracking. This was already observed in other superalloys, such as IN718 [39]. Apparently, the stronger oxidized surface, and thus thicker oxide layers and deeper penetration (Figure 6c), facilitates more cracking if the pronounced precipitation of the γ' phase increases the strength and reduces the formability of the bulk material such that the crack propagation starting from the oxides cannot be hampered.

Therefore, the temperature range of the rolling or forging process of CoWAlloy1 is limited. The materials and deformation temperature should be above or at about that of the γ' solvus temperature due it resulting in a better formability and absent cracking. However, an upper critical temperature for the materials does also exist, since at very high annealing temperatures, the surface is damaged by severe oxidation after longer exposure times, which also facilitates cracking if the temperature at the surface of the material falls below the precipitation temperature of the γ' phase.

5. Conclusions

The present study reveals the origins of crack formation and limited formability during high temperature deformation of the polycrystalline CoNi-base superalloy CoWAlloy1. The following conclusions can be drawn:

- CoWAlloy1 has a high strength and a limited formability below the γ' solvus temperature;
- Cracking and a highly deformed microstructure occur at lower deformation temperatures, while recrystallization and no cracking occurs at higher deformation temperatures that are above that of the γ' solvus temperature;
- Precipitation of the hardening γ' phase is responsible for the high strength and cracking susceptibility;
- Stronger oxidized surfaces at a higher pre-heating temperature seem to lead to more cracking;
- SANS reveals a γ' precipitate radius of about 14 nm for the secondary precipitates and 3 nm for the tertiary precipitates and a total volume fraction of about 62% after cooling down from 1075 °C to 750 °C;
- The combination of different analytical methods optimized on various length scales provides the understanding of the deformation mechanism and possible cracking.

Supplementary Materials: The following supporting information can be downloaded at: https://www.mdpi.com/article/10.3390/met12091520/s1, Figure S1: True stress as a function of true plastic strain at a pre-heating temperature of 1100 °C and different strain rates.

Author Contributions: Conceptualization, S.N.; methodology, S.N.; investigation, D.H., L.P.F., C.S., S.G., R.G. and S.N.; data curation, D.H. and C.S.; writing—original draft preparation, D.H. and L.P.F.; writing—review and editing, M.G., R.G. and S.N.; project administration, S.N.; funding acquisition, M.G., R.G. and S.N. All authors have read and agreed to the published version of the manuscript.

Funding: This research received no external funding.

Institutional Review Board Statement: Not applicable.

Informed Consent Statement: Not applicable.

Data Availability Statement: Not applicable.

Acknowledgments: The authors acknowledge the funding support by the Federal Ministry of Education and Research (BMBF) through the project "An innovative testing machine for heating, quenching, tension, compression and cracking studies of industrial relevant high-temperature alloys-HiMat" (project number 05K19WEC and 05K19WO7).

Conflicts of Interest: The authors declare no conflict of interest.

References

1. Monajati, H.; Taheri, A.K.; Jahazi, M.; Yue, S. Deformation Characteristics of Isothermally Forged UDIMET 720 Nickel-Base Superalloy. *Metall. Mat. Trans. A* **2005**, *36*, 895–905. [CrossRef]

2. Park, N.K.; Kim, I.S.; Na, Y.S.; Yeom, J.T. Hot Forging of a Nickel-Base Superalloy. *J. Mater. Process. Technol.* **2001**, *111*, 98–102. [CrossRef]
3. Guo, S.; Li, D.; Guo, Q.; Wu, Z.; Peng, H.; Hu, J. Investigation on Hot Workability Characteristics of Inconel 625 Superalloy Using Processing Maps. *J. Mater. Sci.* **2012**, *47*, 5867–5878. [CrossRef]
4. Xu, W.; Zhang, L.; Gu, S.; Zhang, J. Hot Compressive Deformation Behavior and Microstructure Evolution of HIPed FGH96 Superalloy. *Trans. Nonferrous Met. Soc. China* **2012**, *22*, 66–71. [CrossRef]
5. Devaux, A.; Georges, E.; Héritier, P. Development of New C&W Superalloys for High Temperature Disk Applications. *AMR* **2011**, *278*, 405–410. [CrossRef]
6. Devaux, A.; Picque, B.; Gervais, M.; Georges, E.; Poulain, T.; Heritier, P. AD730TM-A New Nickel-Based Superalloy for High Temperature Engine Rotative Parts. In Proceedings of the Superalloys 2012 Twelfth International Symposium, Champion, PA, USA, 9–13 September 2012; John Wiley & Sons, Inc.: Hoboken, NJ, USA, 2012; pp. 911–919.
7. Fedorova, T.; Rösler, J.; Klöwer, J.; Gehrmann, B. Development of a New 718-Type Ni-Co Superalloy Family for High Temperature Applications at 750 °C. *MATEC Web Conf.* **2014**, *14*, 01003. [CrossRef]
8. Bergner, M.; Rösler, J.; Gehrmann, B.; Klöwer, J. Effect of Heat Treatment on Microstructure and Mechanical Properties of VDM Alloy 780 Premium. In *Proceedings of the 9th International Symposium on Superalloy 718 & Derivatives: Energy, Aerospace, and Industrial Applications*; Ott, E., Liu, X., Andersson, J., Bi, Z., Bockenstedt, K., Dempster, I., Groh, J., Heck, K., Jablonski, P., Kaplan, M., et al., Eds.; The Minerals, Metals & Materials Series; Springer International Publishing: Cham, Switzerland, 2018; pp. 489–499. ISBN 978-3-319-89479-9.
9. Kümmel, F.; Kirchmayer, A.; Solís, C.; Hofmann, M.; Neumeier, S.; Gilles, R. Deformation Mechanisms in Ni-Based Superalloys at Room and Elevated Temperatures Studied by In Situ Neutron Diffraction and Electron Microscopy. *Metals* **2021**, *11*, 719. [CrossRef]
10. Lass, E.A.; Williams, M.E.; Campbell, C.E.; Moon, K.-W.; Kattner, U.R. γ' Phase Stability and Phase Equilibrium in Ternary Co-Al-W at 900 °C. *J. Phase Equilib. Diffus.* **2014**, *35*, 711–723. [CrossRef]
11. Knop, M.; Mulvey, P.; Ismail, F.; Radecka, A.; Rahman, K.M.; Lindley, T.C.; Shollock, B.A.; Hardy, M.C.; Moody, M.P.; Martin, T.L.; et al. A New Polycrystalline Co-Ni Superalloy. *JOM* **2014**, *66*, 2495–2501. [CrossRef]
12. Neumeier, S.; Freund, L.P.; Göken, M. Novel Wrought γ/γ' Cobalt Base Superalloys with High Strength and Improved Oxidation Resistance. *Scr. Mater.* **2015**, *109*, 104–107. [CrossRef]
13. Titus, M.S.; Eggeler, Y.M.; Suzuki, A.; Pollock, T.M. Creep-Induced Planar Defects in L12-Containing Co- and CoNi-Base Single-Crystal Superalloys. *Acta Mater.* **2015**, *82*, 530–539. [CrossRef]
14. Sani, S.A.; Arabi, H.; Kheirandish, S.; Ebrahimi, G. Investigation on the Homogenization Treatment and Element Segregation on the Microstructure of a γ/γ'-Cobalt-Based Superalloy. *Int. J. Min. Met. Mater* **2019**, *26*, 222–233. [CrossRef]
15. Freund, L.P.; Giese, S.; Schwimmer, D.; Höppel, H.W.; Neumeier, S.; Göken, M. High Temperature Properties and Fatigue Strength of Novel Wrought γ/γ' Co-Base Superalloys. *J. Mater. Res.* **2017**, *32*, 4475–4482. [CrossRef]
16. Freund, L.P.; Stark, A.; Pyczak, F.; Schell, N.; Göken, M.; Neumeier, S. The Grain Boundary Pinning Effect of the μ Phase in an Advanced Polycrystalline γ/γ' Co-Base Superalloy. *J. Alloys Compd.* **2018**, *753*, 333–342. [CrossRef]
17. Churyumov, A.Y.; Medvedeva, S.V.; Mamzurina, O.I.; Kazakova, A.A.; Churyumova, T.A. United Approach to Modelling of the Hot Deformation Behavior, Fracture, and Microstructure Evolution of Austenitic Stainless AISI 316Ti Steel. *Appl. Sci.* **2021**, *11*, 3204. [CrossRef]
18. Yao, D.; Cai, L.; Bao, C. A New Fracture Criterion for Ductile Materials Based on a Finite Element Aided Testing Method. *Mater. Sci. Eng. A* **2016**, *673*, 633–647. [CrossRef]
19. Evans, R.W. Modelling of the Hot-Working of High Perfomance Alloys. *KEM* **1992**, *77–78*, 227–240. [CrossRef]
20. Jaramillo, R.A.; Suarez, F.S.; Plyburn, J.A.; Camus, D.E. Evaluation of an Inconel Alloy 718 Microstructural Evolution Model. In Proceedings of the Superalloys 718, 625, 706 and Various Derivatives (1997), Pittsburgh, PA, USA, 15–18 June 1997; TMS: Pittsburgh, PA, USA, 1997; pp. 257–266.
21. Brooks, J.W. Forging of Superalloys. *Mater. Des.* **2000**, *21*, 297–303. [CrossRef]
22. Dandre, C.A.; Walsh, C.A.; Evans, R.W.; Reed, R.C.; Roberts, S.M. Microstructural Evolution of Nickel-Base Superalloy Forgings during Ingot-to-Billet Conversion: Process Modeling and Validation. In Proceedings of the Superalloys 2000 (Ninth International Symposium), Seven Springs, PA, USA, 17–21 September 2000; TMS: Pittsburgh, PA, USA, 2000; pp. 85–94.
23. Zhang, H.Y.; Zhang, S.H.; Li, Z.X.; Cheng, M. Hot Die Forging Process Optimization of Superalloy IN718 Turbine Disc Using Processing Map and Finite Element Method. *Proc. Inst. Mech. Eng. Part B J. Eng. Manuf.* **2010**, *224*, 103–110. [CrossRef]
24. Gilles, R.; Mukherji, D.; Eckerlebe, H.; Strunz, P.; Rösler, J. *In Situ* Investigation with Neutrons on the Evolution of γ' Precipitates at High Temperatures in a Single Crystal Ni-Base Superalloy. *AMR* **2011**, *278*, 42–47. [CrossRef]
25. Collins, D.M.; Heenan, R.K.; Stone, H.J. Characterization of Gamma Prime (γ') Precipitates in a Polycrystalline Nickel-Base Superalloy Using Small-Angle Neutron Scattering. *Metall. Mat. Trans. A* **2011**, *42*, 49–59. [CrossRef]
26. Del Genovese, D.; Rösler, J.; Strunz, P.; Mukherji, D.; Gilles, R. Microstructural Characterization of a Modified 706-Type Ni-Fe Superalloy by Small-Angle Neutron Scattering and Electron Microscopy. *Metall. Mat. Trans. A* **2005**, *36*, 3439–3450. [CrossRef]
27. Mukherji, D.; Del Genovese, D.; Strunz, P.; Gilles, R.; Wiedenmann, A.; Rösler, J. Microstructural Characterisation of a Ni–Fe-Based Superalloy by *in Situ* Small-Angle Neutron Scattering Measurements. *J. Phys. Condens. Matter* **2008**, *20*, 104220. [CrossRef]

28. Ratel, N.; Bruno, G.; Demé, B. *In Situ* Small-Angle Neutron Scattering Investigation of the γ' Precipitation and Growth in the Nickel-Based Single-Crystal Alloy SC16. *J. Phys. Condens. Matter* **2005**, *17*, 7061–7075. [CrossRef]
29. Hausmann, D.; Solís, C.; Freund, L.P.; Volz, N.; Heinemann, A.; Göken, M.; Gilles, R.; Neumeier, S. Enhancing the High-Temperature Strength of a Co-Base Superalloy by Optimizing the γ/γ' Microstructure. *Metals* **2020**, *10*, 321. [CrossRef]
30. Wan, Z.; Hu, L.; Sun, Y.; Wang, T.; Li, Z. Hot Deformation Behavior and Processing Workability of a Ni-Based Alloy. *J. Alloys Compd.* **2018**, *769*, 367–375. [CrossRef]
31. Schneider, C.A.; Rasband, W.S.; Eliceiri, K.W. NIH Image to ImageJ: 25 Years of Image Analysis. *Nat. Methods* **2012**, *9*, 671–675. [CrossRef]
32. Mühlbauer, S.; Heinemann, A.; Wilhelm, A.; Karge, L.; Ostermann, A.; Defendi, I.; Schreyer, A.; Petry, W.; Gilles, R. The New Small-Angle Neutron Scattering Instrument SANS-1 at MLZ—Characterization and First Results. *Nucl. Instrum. Methods Phys. Res. Sect. A Accel. Spectrometers Detect. Assoc. Equip.* **2016**, *832*, 297–305. [CrossRef]
33. Gilles, R. How Neutrons Facilitate Research into Gas Turbines and Batteries from Development to Engineering Applications. *J. Synch. Investig.* **2020**, *14*, S69–S74. [CrossRef]
34. Keiderling, U. The New "BerSANS-PC" Software for Reduction and Treatment of Small Angle Neutron Scattering Data. *Appl. Phys. A Mater. Sci. Process.* **2002**, *74*, s1455–s1457. [CrossRef]
35. Breßler, I.; Kohlbrecher, J.; Thünemann, A.F. *SASfit*: A Tool for Small-Angle Scattering Data Analysis Using a Library of Analytical Expressions. *J. Appl. Crystallogr.* **2015**, *48*, 1587–1598. [CrossRef] [PubMed]
36. Freund, L.P. Mikrostrukturelle Und Mechanische Charakterisierung von Polykristallinen Ausscheidungsgehärteten Co-Basis Superlegierungen Unter Besonderer Berücksichtigung Der Verformungsmechanismen. Ph.D. Thesis, Friedrich-Alexander-Universität Erlangen-Nürnberg, Erlangen, Germany, 2019.
37. Porter, D.A.; Easterling, K.E.; Sherif, M.Y. *Phase Transformations in Metals and Alloys*, 3rd ed.; CRC Press: Boca Raton, FL, USA, 2009; ISBN 978-1-4200-6210-6.
38. Haynes. Available online: https://www.hpalloy.com/Alloys/descriptions/HAYNES25.aspx (accessed on 16 November 2021).
39. Krupp, U.; Kane, W.M.; Laird, C.; McMahon, C.J. Brittle Intergranular Fracture of a Ni-Base Superalloy at High Temperatures by Dynamic Embrittlement. *Mater. Sci. Eng. A* **2004**, *387–389*, 409–413. [CrossRef]